

A Fine-Grained Attention and Geometric Correspondence Model for Musculoskeletal Risk Classification in Athletes Using Multimodal Visual and Skeletal Features

Md. Abdur Rahman^{1,a}, Mohaimenul Azam Khan Raiaan^{1,a}, Tamanna Shermin¹,
Md Rafiqul Islam², Mukhtar Hussain², Sami Azam^{2,*}

¹Department of Computer Science and Engineering, United International University, Dhaka 1212, Bangladesh

²Faculty of Science and Technology, Charles Darwin University, Australia

^aEqual Contributions

*Corresponding Author: sami.azam@cdu.edu.au

Abstract

Musculoskeletal disorders pose significant risks to athletes, and assessing risk early is important for prevention. However, most existing methods are designed for controlled settings and fail to reliably assess risk in complex environments due to their reliance on a single type of data. This research introduces ViSK-GAT (Visual-Skeletal Geometric Attention Transformer), a novel multimodal deep learning framework that classifies musculoskeletal risk using both visual and skeletal coordinate-based features. A custom multimodal dataset (MusDis-Sports) was created by combining images and skeletal coordinates, with each sample labeled into eight risk categories based on the Rapid Entire Body Assessment (REBA) system. ViSK-GAT integrates two innovative modules: the Fine-Grained Attention Module (FGAM), which refines inter-modal features via cross-attention between visual and skeletal inputs, and the Multimodal Geometric Correspondence Module (MGCM), which enhances cross-modal alignment between image features and coordinates. The model achieved robust performance, with all key metrics exceeding 93%. Regression results also indicated a low RMSE of 0.1205 and MAE of 0.0156. ViSK-GAT consistently outperformed nine popular transfer learning backbones and showed its potential to advance AI-driven musculoskeletal risk assessment and enable early, impactful interventions in sports.

Keywords: Deep Learning; REBA; Musculoskeletal Risk; Posture Recognition; Multimodal Framework; Fine-Grained Attention

1 Introduction

Musculoskeletal disorders (MSD) are among the main concerns in athletic performance, which pose significant risks that can affect movement efficiency, endurance, and long-term health [1]. These disorders arise from repetitive strain, improper biomechanics, and sustained postural imbalances, leading to muscle fatigue, joint stress, and chronic injuries [2]. Given these challenges, posture plays an important role in athletes' performance, endurance, and injury prevention. Proper posture improves balance, stability, and coordination, key factors in executing precise movements. In contrast, poor posture can cause muscle imbalances and an increased risk of musculoskeletal injuries, such as strains, sprains, and joint stress [3]. Therefore, effective movement management is essential not only for athletes but for individuals of all ages and levels of activity, as it supports long-term health, safety, and overall well-being [4]. Researchers have continuously sought ways to design more effective training

environments and develop techniques that recognize movements [5]. However, addressing these risks requires a proactive approach to posture monitoring and correction, where sports ergonomics becomes essential. Despite their levels of athleticism, many athletes experience postural disturbances due to repetitive training [6, 7], eventually leading to musculoskeletal degeneration and chronic conditions [8, 9].

Several biomechanical assessment methods have been introduced to assess posture and the risk of work-related musculoskeletal disorders (WMSD). These include the Rapid Entire Body Assessment (REBA) [10], Rapid Upper Limb Assessment (RULA) [11], Ovako Working posture Analysis System (OWAS) [12], Manual Material Handling (MMH) [13], Occupational Repetitive Action (OCRA) [17], etc. These methods quantitatively analyze human postures to improve the reliability and precision of assessments. Although originally developed for occupational ergonomics, several studies reinforce the adaptation of these methods

(e.g., REBA) from industrial ergonomics into athletic contexts [14]. Moreover, these have been effectively applied to the sports environment as well. For example, Kazemi et al. [15] applied REBA to Physical Education students, linking postural risks with musculoskeletal disorders, while Gorce et al. [16] used it to quantify injury risks during the tennis serve.

Recently, posture assessment has increasingly transitioned into the automation phase. For example, sensor-based methods [18, 19, 20] provide the advantage of continuous monitoring, while computer vision-based approaches [21, 22, 23, 45] offer non-invasive alternatives. More recently, multimodal methods [25, 26, 27] have emerged to integrate complementary data types for posture evaluation. Although existing models have shown success in workplace ergonomics and human activity recognition, they often fail to address the unique challenges present in sports environments. Many systems struggle with real-time adaptability, occlusions during dynamic movements, and the effective integration of multimodal data sources. Furthermore, issues such as signal instability, calibration sensitivity, and discomfort caused by monitoring devices can interfere with the natural performance of an athlete [28, 29]. Capturing dynamic posture changes in fast-paced sports remains difficult, as environmental factors such as occlusion and limited field of view can hinder reliable evaluations [21, 22]. Although some approaches aim to combine multiple data sources, they often fail to effectively align and integrate various types of information, especially under rapidly changing conditions [25, 26]. Furthermore, many models were designed for controlled settings, which limits their applicability to the dynamic real-world environment [30, 27]. These challenges highlight the need for a more adaptable system capable of providing precise real-time posture assessments in athletic environments.

Thus, to address these critical limitations, we propose ViSK-GAT (Visual-Skeletal Geometric Attention Transformer), a multimodal framework designed for robust and interpretable posture risk assessment in athletic environments. While cross-attention is an established mechanism for multimodal fusion, its standard application often treats modalities as monolithic blocks for global alignment. This can be suboptimal for fine-grained postural analysis, where specific local image features (e.g., a bent elbow) must be precisely correlated with specific skeletal keypoints. To address this, ViSK-GAT introduces a structured, two-stage attention pipeline. The Fine-Grained Attention Module (FGAM) first performs intra-modal refinement, enhancing discriminative local features within the image data before fusion. This prepared representation is then processed by the Multimodal Geometric Correspondence Module (MGCM), which performs a spatially-aware cross-modal alignment. Unlike generic cross-attention, MGCM is designed explicitly

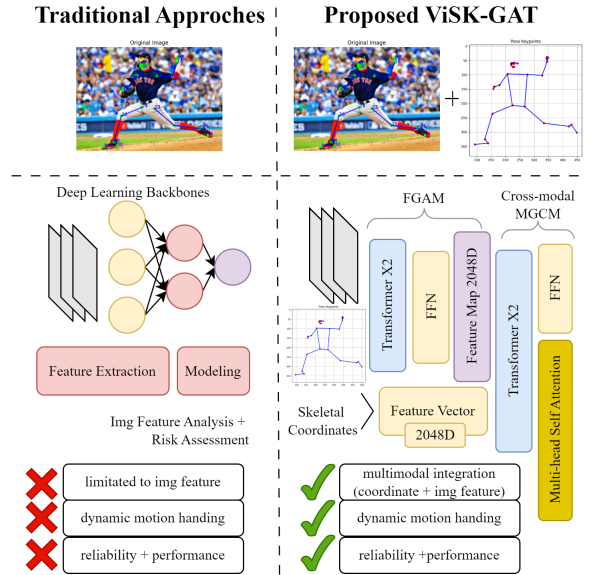


Figure 1: We processed the img feature with Fine-Grained Attention Module (FGMA) and used a coordinate feature encoder for skeletal feature processing. The Multimodal Geometric Correspondence Module (MGCM) uses a cross-attention mechanism for the image and coordinate feature integration and risk assessment.

to bridge the domain gap between visual texture and geometric coordinate spaces, ensuring that the model’s fusion is grounded in the biomechanical reality of the human body.

Furthermore, unlike conventional approaches (see Figure 1) that struggle under real-world conditions, ViSK-GAT effectively combines high-level visual features with fine-grained skeletal data, enabling accurate posture classification even during dynamic movements and partial occlusion. Our extensive evaluations highlight the superiority of ViSK-GAT, which achieves a test accuracy of 93.89%, significantly outperforming state-of-the-art backbones, even when these models are paired with identical fusion and classification pipelines. Compared to previous studies on ergonomic risk assessment, ViSK-GAT demonstrates leading and competitive performance. Although prior models using ergonomic metrics such as OWAS and RULA report test accuracies ranging from 76.10% to 93.00%, ViSK-GAT surpasses these with a test accuracy of 93.89%, also using the more fine-grained and anatomically detailed REBA scoring system, which is better suited for dynamic posture analysis in sports. These results collectively establish ViSK-GAT as a great solution, both in terms of accuracy and architectural innovation, for multimodal ergonomic risk assessment, particularly in the complex and fast-paced conditions of athletic environments.

The major contributions of our work are as follows:

- A comprehensive multimodal annotated dataset is

constructed by integrating multiple sports datasets and extracting human skeletal coordinates using MediaPipe.

- A novel multimodal system is proposed that integrates visual and coordinate-based data to enhance the accuracy of the risk classification of musculoskeletal disorders in athletes, using REBA-based posture scoring as the core evaluation framework.
- A hybrid backbone is developed using Residual Blocks and Lightweight Transformer Blocks to extract features for efficient posture analysis in sports.
- A Fine-Grained Attention Module is introduced to enhance multimodal feature processing through a cross-attention mechanism and improve the interaction between image-based and coordinate-based features for more precise risk assessment.
- A Multimodal Geometric Correspondence Module is designed using a transformer-based framework to align images and coordinate features to ensure accurate representations of an athlete’s posture despite occlusions and perspective distortions.

The rest of the paper is organized as follows: Section 2 reviews related works on musculoskeletal disorder risk assessment with vision-based and multimodal approaches. Section 3 describes the methodology, including the construction of the MusDis-Sports dataset and the design of the proposed multimodal framework. Section 4 presents the experimental results, detailing the classification outcomes, configuration analysis, and comparison with recent studies. Section 5 presents a discussion of the findings and their implications. Section 6 outlines the limitations and proposes directions for future research, and finally, Section 7 summarizes the main contributions and results of the study.

2 Related works

Numerous methods have been developed to help ergonomists assess the risks of Musculoskeletal Disorders (MSD). Traditional approaches, such as the Ovako Working posture Analysis System (OWAS), the Rapid Entire Body Assessment (REBA), the Musculoskeletal Disorders (MSD) Checklist, and the Rapid Upper Limb Assessment (RULA), have been widely adopted but often rely on manual scoring by ergonomic experts. Recently, modern technology has enabled the integration of modern monitoring devices into MSDs’ risk assessments.

2.1 Vision-based methods

Vision-based methods mostly use deep learning networks to analyze human activities with potential MSD risks in a

non-invasive way. In the study of Li et al. [21], a vision-based real-time method was proposed to assess postural risk factors for musculoskeletal disorders using CNN feature extraction to generate 2D postures. The algorithm achieved 93% accuracy in detecting RULA action levels. On the other hand, Kim et al. [22] adopted an open-source technology named OpenPose to develop a human pose estimation system. The system counted the angles of each part of the body from a two-dimensional perspective to assess the level of risk of posture. Seo et al. [23] introduced a computer vision-based method for the automatic identification of construction worker postures to assess ergonomic risk. Using classification techniques to learn from various postures depicted in virtual images, they achieved 89% precision in classifying diverse postures in the images. In another study, Dzung et al. [31] proposed an approach that automatically tracks and categorizes postures based on OWAS using skeleton-based motion data to analyze ergonomic risks. The posture identification accuracies exceeded 90% for most activities, with up to 88.5% in the OWAS assessment. On the same assessment (i.e, OWAS), Yan et al. [32] achieved a maximum accuracy of 89.2% using three posture classifiers for construction hazard prevention. Many researchers have also proposed ergonomic assessment based on skeletons extracted either from 2D images from an ordinary camera or 3D images produced by RGB-D sensors [32, 33, 34, 35, 45].

2.2 Multimodal-based methods

While vision-based methods individually contribute valuable insights into MSD risk assessment, recent advances have considered the potential of combining multiple data modalities for posture recognition.

For instance, Xiahou et al. [25] proposed a feature-level fusion framework that integrates signals from various sensors using deep learning models such as multilayer perceptrons (MLPs), recurrent neural networks (RNNs), and long short-term memory (LSTM) networks. Their LSTM-based model maintained over 90% accuracy even under adverse environmental conditions. Similarly, Zhao et al. [26] designed a multimodal bioinformation fusion algorithm that extracted motion features from both hand and leg movements using wavelet packet decomposition and sample entropy. Their method achieved recognition rates consistently above 95%. Several studies have also combined visual and sensor data for posture and behavior recognition. For instance, Zhang et al. [27] introduced a deep learning framework that fuses infrared and pressure map data to recognize sitting postures. Using modality-specific backbones and a cross-modal self-attention mechanism, they achieved an F1-score of 93.08%. Furthermore, Palash et al. [36] introduced a modular two-stream CNN and RNN framework that fuses facial expressions, body posture, and gait features early, while utilizing situational knowledge to enhance multimodal emotion recognition. Meanwhile, Qi et al. [37] introduced



Figure 2: Sample images from the constructed MusDis-Sports dataset showing athletes in various sports-related postures with overlaid 2D skeletal keypoints extracted using the MediaPipe framework. These samples are used for training and evaluating musculoskeletal risk classification.

a federated learning-based multimodal framework for fall detection, where time-series data from wearable sensors and visual data from cameras are fused at the input level using a Gramian Angular Field transformation. Their model reached up to accuracies of 99.927% and 89.769% for binary and multi-class fall activity recognition tasks, respectively. Similarly, Liu et al. [38] developed a hydrogel-based system for monitoring respiration and recognizing finger-pressing postures. Even though they achieved a posture recognition accuracy of 99.259%, their work primarily relied on a wearable sensor system, which often adds additional inconvenience to the users.

Despite the notable advancements, existing studies still show drawbacks. For instance, vision-based methods, although non-invasive, often suffer from challenges such as limited camera coverage, occlusion, and sensitivity to environmental factors like lighting, which makes the posture recognition tasks less reliable in dynamic, fast-paced environments like sports. Even though the multimodal approaches have shown potential, many rely on handcrafted fusion strategies and often lack fine-grained integration between modalities. Moreover, a significant portion of prior studies focus on specific activities or controlled environments, which reduces their applicability to diverse real-world settings. In this work, we propose a novel multimodal system that integrates both visual and coordinate-based data through fine-grained attention and geometric correspondence mechanisms and offers a more accurate and generalizable approach for musculoskeletal disorder (MSD) risk assessment in athletes.

3 Methodology

This section details our dataset construction with coordinate extraction and REBA-based risk annotation, along with the design of our ViSK-GAT, consisting of a hybrid backbone, attention module, and geometric alignment.

3.1 MusDis-Sports dataset

To facilitate the training and evaluation of our proposed multimodal ergonomic risk assessment model, we constructed a domain-specific dataset (MusDis-Sports) for posture analysis in athletic scenarios. The image data were compiled from various publicly available sports datasets, including Sports-1M [39], Sports Classification [40], Sports Image Classification [41], and the Cricket Shot [42] datasets. These sources were selected for their diversity in body configurations, motion states, and camera viewpoints to capture a wide range of postures.

Our MusDis-Sports dataset comprises 8989 annotated samples, each consisting of an image of a human subject in a sports-related posture, the corresponding 2D skeletal keypoints, and an ergonomically informed class label representing the REBA-based risk category. Figure 2 visualizes some images from the constructed dataset. The dataset can be accessed through the footnoted GitHub repository¹.

3.1.1 Image and skeleton coordinate construction

In this study, we curated a dataset (MusDis-Sports) of ergonomic postures in athletic contexts by selecting only those samples from publicly available sports datasets. In our study, only images with visible full-body configurations were retained. Each selected image was processed through the MediaPipe framework [43] to extract body landmarks. MediaPipe was selected as the pose estimation framework for this study due to its status as a widely adopted, open-source standard that provides a scalable and reproducible method for generating skeletal keypoints, which is necessary for large-scale dataset creation. This framework outputs 33 anatomical keypoints corresponding to major joints and body segments. For every subject present in an image, MediaPipe’s pretrained model was used to extract 33 anatomical landmarks per subject, defined in Equation (1):

$$\mathcal{K} = \{(x_i, y_i, v_i)\}_{i=1}^{33}, \quad (x_i, y_i) \in [0, 1]^2, \quad v_i \in [0, 1] \quad (1)$$

¹https://github.com/mak-raiaan/MusDis-Sports_Dataset

where (x_i, y_i) denote normalized 2D coordinates for landmark i , and v_i represents the visibility confidence of that point. We filtered out unreliable landmarks by excluding any keypoint with $v_i < 0.5$. The remaining coordinates were scaled to the original image dimensions, forming the 2D skeletal matrix $K \in \mathbb{R}^{33 \times 2}$. To support downstream ergonomic analysis, angular features were extracted from skeletal keypoint triplets using two complementary methods.

First, we calculated the joint angles using the cosine law. For any three keypoints A , B , and C , the the forming joint angle at B was computed as shown in Equation (2):

$$\theta_{ABC} = \cos^{-1} \left(\frac{(\vec{BA} \cdot \vec{BC})}{|\vec{BA}| \cdot |\vec{BC}|} \right) \quad (2)$$

where $\vec{BA} = A - B$ and $\vec{BC} = C - B$ are vectors formed from the coordinates of the three points, and $\|\cdot\|$ denotes the Euclidean norm. With this, the angular displacement at joints such as the elbow, knee, or shoulder was computed.

Second, vertical inclination angles were computed to assess postural deviations like trunk or neck flexion. These were derived using a slope-based formulation that calculates the angular deviation from the vertical axis. For example, the trunk tilt angle θ_{trunk} between the shoulder and hip centers was given as shown in Equation (3):

$$\theta = \tan^{-1} \left(\frac{|x_{\text{shoulder}} - x_{\text{hip}}| + \epsilon}{|y_{\text{shoulder}} - y_{\text{hip}}|} \right) \quad (3)$$

where $(x_{\text{shoulder}}, y_{\text{shoulder}})$ and $(x_{\text{hip}}, y_{\text{hip}})$ denote the 2D coordinates of the shoulder and hip midpoints, respectively. The small constant ϵ is included to prevent division by zero in near-vertical poses. Algorithm 1 presents the overall process of extracting coordinates and calculating angles from a set of input images.

3.1.2 REBA labeling

We computed ergonomic risk scores using a structured implementation of the REBA protocol, following the methodology proposed by Hignett and McAtamney [10]. It is a standardized tool for evaluating the risk of musculoskeletal disorders based on body posture and has been widely used in ergonomics and occupational health studies [44]. The process involves segmenting the human body into functional regions (e.g., trunk, neck, legs, upper arms, lower arms, and wrists) and assigning each part a discrete risk score based on the estimated joint angles.

In our work, once the angular displacements for relevant joints were computed (see Section 3.1.1), we assigned region-specific scores based on angle thresholds inspired by the REBA guidelines. It is important to note that the REBA scores are generated by applying a deterministic, rule-based algorithm to the coordinates. The model’s task is therefore

Algorithm 1 Skeleton Coordinate Extraction and Angle Calculation Process

```

1: Input: images  $\mathcal{I} = \{I_1, I_2, \dots, I_N\}$ 
2: for each image  $I \in \mathcal{I}$  do
3:   Apply MediaPipe to keypoints:  $\mathcal{K} = \{(x_i, y_i, v_i)\}_{i=1}^{33}$ 
4:   Initialize empty keypoint list  $\mathbf{K}$ 
5:   for each keypoint  $(x_i, y_i, v_i) \in \mathcal{K}$  do
6:     if  $v_i \geq 0.5$  then
7:       Rescale  $(x_i, y_i)$  to original image size
8:       Append to  $\mathbf{K}$ 
9:     end if
10:  end for
11:  for each joint triplet  $(A, B, C)$  in  $\mathbf{K}$  do
12:    vectors:  $\vec{BA} \leftarrow A - B$ ,  $\vec{BC} \leftarrow C - B$ 
13:    angles: compute angle  $\theta_{ABC}$ 
14:  end for
15:  for each body segment do
16:    v_angel: vertical inclination angle  $\theta$ 
17:  end for
18:  Overlay keypoints and skeletal edges on image  $I$ 
19:  Save the annotated image
20: end for

```

to learn the mapping from visual and coordinate data to the output of this function, not to the raw MediaPipe coordinates themselves. We used a group-based formulation [10] in which the trunk, neck, and leg scores were aggregated to derive the Group A score, while the upper arm, lower arm, and wrist scores were combined to obtain the Group B score. These two group scores were subsequently mapped to a final REBA risk level through a predefined matrix, corresponding to the Group C scoring table outlined in the original REBA protocol.

Our study specifically focuses on the 6 body parts: neck, trunk, wrist, upper arm, lower arm, and legs. As our dataset consists of single-frame images without dynamic tasks or load handling, we fixed both the load and activity modifiers to zero. The final Group C value was treated as the REBA scores, and based on the final calculated scores, we defined 8 classes, where classes with a higher number (i.e., 4+) indicate riskier postures. Table 1 reports the dataset samples and ratio in terms of eight classes.

Although some REBA protocol relies on 3D angular measurements, we employed a 2D approximation for broader applicability in conventional available image data that preserves the relative ranking of joint stresses. The resulting classes, therefore, represent postural intensity levels derived from 2D angular displacements. This reinterpretation ensures the labels remain meaningful even within monocular visual data. To ensure labeling reliability despite the automatic nature of REBA score generation, (i) we used MediaPipe’s built-in visibility confidence scores to exclude

Table 1: Class-wise distribution of annotated samples in the proposed MusDis-Sports dataset. Higher REBA classes (e.g., Class 4–8) indicate riskier postures associated with greater musculoskeletal disorder risk.

REBA Class	Samples	Ratio (approx.)
Class 1	1083	12.05%
Class 2	1213	13.49%
Class 3	1181	13.14%
Class 4	1332	14.82%
Class 5	1144	12.73%
Class 6	1117	12.43%
Class 7	888	09.88%
Class 8	1031	11.47%
Total	8989	100%

low-certainty landmarks ($vi < 0.7$); (ii) for each body-region score, we analyzed internal consistency by correlating the derived angular magnitudes across overlapping joints (e.g., shoulder–elbow–wrist chains) and retained samples with consistent geometry; and (iii) Furthermore, to assess labeling stability, we performed a manual sanity check on a random subset of 500 images to visually confirm that the overlay of skeletal keypoints was accurate and that the assigned REBA class was plausible given the posture. We also processed the samples under slightly varied viewing scales and compared them using the intraclass correlation coefficient ($ICC = 0.84$). Our findings indicate that the automatically derived REBA labels are self-consistent within a reasonable tolerance for 2D estimation. The REBA score assignment process is briefed in Algorithm 2.

Algorithm 2 REBA Score Assignment from Posture Scores

```

1: Input: Scores:  $s_{neck}$ ,  $s_{trunk}$ ,  $s_{leg}$ ,  $s_{upper}$ ,  $s_{lower}$ ,  $s_{wrist}$ 
2: function GROUPA( $s_{neck}$ ,  $s_{trunk}$ ,  $s_{leg}$ )
3:   use REBA lookup to compute  $g_A$ 
4:   return  $g_A$ 
5: end function
6: function GROUPB( $s_{upper}$ ,  $s_{lower}$ ,  $s_{wrist}$ )
7:   use REBA lookup to compute  $g_B$ 
8:   return  $g_B$ 
9: end function
10: function GROUPC( $g_A$ ,  $g_B$ )
11:    $S_{REBA} \leftarrow \text{table}[g_A][g_B]$ 
12:   return  $S_{REBA}$ 
13: end function
14:  $g_A \leftarrow \text{GROUPA}(s_{neck}, s_{trunk}, s_{leg})$ 
15:  $g_B \leftarrow \text{GROUPB}(s_{upper}, s_{lower}, s_{wrist})$ 
16:  $S_{REBA} \leftarrow \text{GROUPC}(g_A, g_B)$ 
17: return  $S_{REBA}$ 
18: Output: final REBA score,  $S_{REBA}$ 

```

3.2 Proposed model

Our proposed Visual-Skeletal Geometric Attention Transformer (ViSK-GAT) is a novel multimodal architecture that effectively integrates visual and coordinate-based skeletal representations using transformer-enhanced attention mechanisms for robust classification.

The model begins with a custom ResNet-inspired encoder backbone composed of residual blocks to extract high-dimensional visual features from input images. These features are then refined through two core modules that represent the key innovations of our approach. The Fine-Grained Attention Module (detailed in Section 3.2.2) employs multi-head self-attention combined with lightweight transformer blocks to enable precise inter-modal feature refinement. This module enhances the ability of the model to focus on discriminative visual patterns while maintaining spatial consistency through residual connections and layer normalization.

The most significant contribution of the framework is the Multimodal Geometric Correspondence Module (MGCM), which aligns visual features with coordinate-based skeletal representations through cross-attention mechanisms (see Section 3.2.3). MGCM maps both modalities into a shared latent space, where attention-based feature alignment allows the model to learn complex cross-modal correspondences and geometric relationships. This alignment facilitates a coherent understanding of spatial structures and visual semantics. We further enhance the integrated features using a final transformer-based refinement stage (see Section 3.2.1), which captures long-range contextual dependencies across modalities. This leads to a unified and discriminative multimodal representation suitable for complex musculoskeletal risk classification tasks. Figure 3 illustrates the proposed ViSK-GAT framework.

3.2.1 Hybrid multimodal feature extraction

To process both visual and coordinate data, we designed a dual-branch feature extraction backbone that handles the heterogeneity of input modalities. This module takes two distinct types of input: image frames representing the full body posture and the corresponding 2D skeletal keypoints.

First, the image branch operates directly on the image frames. We initially resized all frames to a fixed spatial resolution and passed them through Residual Blocks. We used the residual connections to maintain spatial information across deeper layers. Each residual block refines the image representation without suffering from vanishing gradients, ultimately generating a high-dimensional feature map $F_{\text{img}} \in \mathbb{R}^{H \times W \times C}$, where H and W are the spatial dimensions, and C is the channel depth, respectively.

Parallel to this, the coordinate branch handles structured skeleton data, where each frame contains 33 keypoints representing body joints. Each keypoint has 2D coordinates

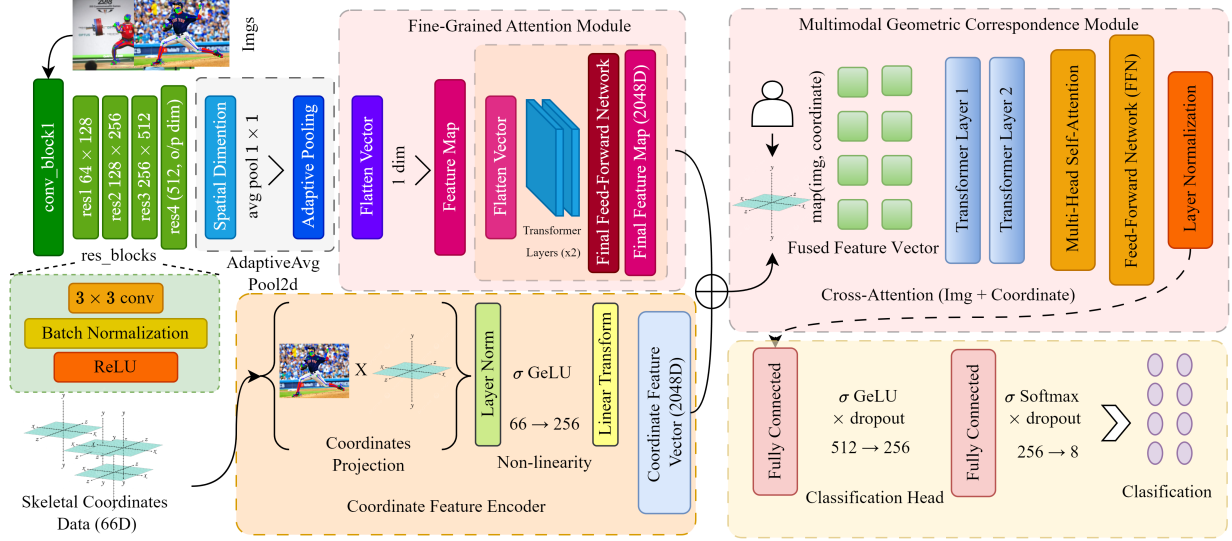


Figure 3: Overview of the proposed multimodal framework (ViSK-GAT) for ergonomic posture risk assessment. The system integrates visual features and skeletal coordinates through a hybrid backbone, enhanced by a Fine-Grained Attention Module and a Multimodal Geometric Correspondence Module.

(x_i, y_i) , normalized to lie within $[0, 1]$. We began by flattening the skeleton into a sequence of joint tokens $P \in \mathbb{R}^{N \times 2}$, which was then projected to a higher-dimensional space using a learnable linear transformation, as shown in Equation (4):

$$E_{\text{pose}} = PW_e + b_e \quad (4)$$

where $W_e \in \mathbb{R}^{2 \times d}$ and $b_e \in \mathbb{R}^d$ are the learned weights and biases for pose embedding, and d is the latent dimension. The resulting tensor $E_{\text{pose}} \in \mathbb{R}^{N \times d}$ represents spatial relationships among joints. Then, to capture higher-order dependencies and long-range interactions between postures, we passed E_{pose} through a lightweight Transformer block, which uses self-attention to model correlations between distant joints and output an enhanced coordinate feature representation, F_{pose} . The Transformer block includes multi-head attention and feed-forward sublayers, allowing the model to learn contextual interactions between joints, such as whether the arms and torso are aligned in a squat or the symmetry of the legs during a lunge.

Finally, the output of both branches (i.e., F_{img} and F_{pose}) formed the basis for cross-modal reasoning in the following modules. We kept these representations distinct at this stage to maintain modality-specific semantics.

3.2.2 Fine-grained attention module

After extracting modality-specific features from the dual branches (i.e., image tokens $F_{\text{img}} \in \mathbb{R}^{256 \times 128}$, and pose embeddings $F_{\text{pose}} \in \mathbb{R}^{33 \times 128}$), we found that the image representation alone was not sufficient to encode subtle postural variations relevant for risk classification. Although the backbone extracted general visual features effectively,

it lacked contextual focus on regions important for posture interpretation, such as limb orientation or joint symmetry.

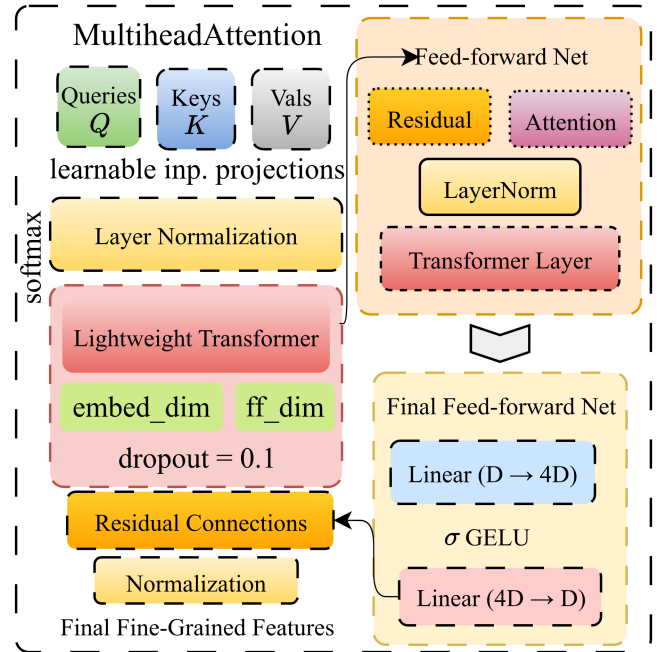


Figure 4: Architecture of the proposed Fine-Grained Attention Module for enhancing token representations.

To address this, we introduced a Fine-Grained Attention Module (FGAM) for refining the token sequence (see Figure 4). Our goal was to let each image patch attend to others within the same modality and enhance discriminative posture cues before engaging in cross-modal fusion.

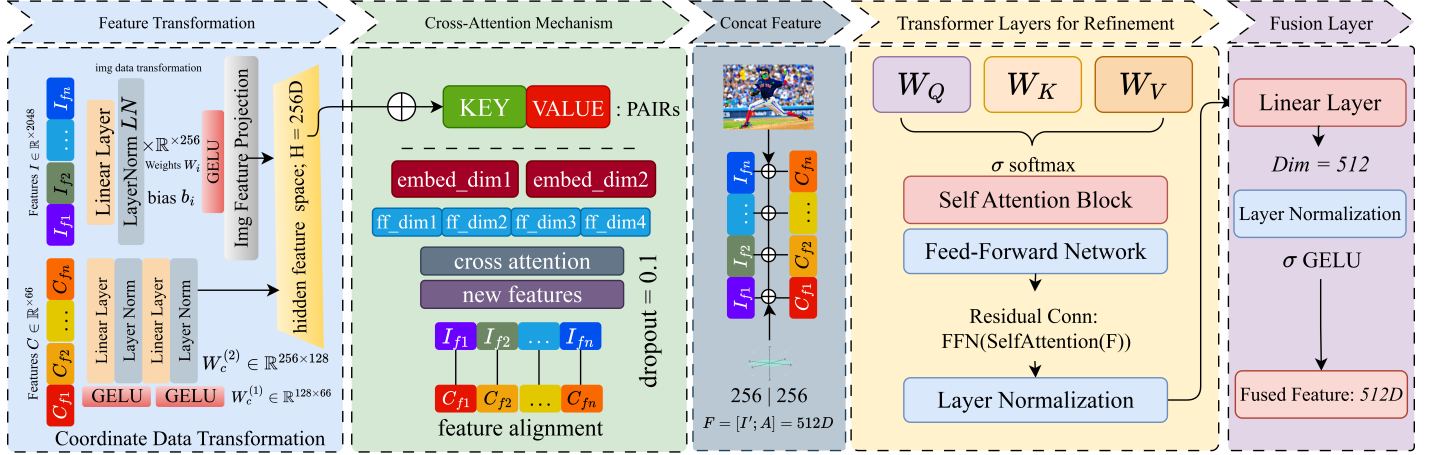


Figure 5: Proposed architecture of the Multimodal Geometric Correspondence Module (MGCM). This is a cross-attention transformer designed to bridge the gap between image tokens (Query) and skeletal coordinate embeddings (Key and Value). The process involves: (1) projecting both features into a common latent space; (2) using cross-attention to align visual appearance with structural posture information; (3) concatenating the attention output with the image feature; and (4) refining the combined feature using stacked Transformer layers to produce the final Fused Feature Vector (F_{corr}) for risk classification.

We began by passing F_{img} through a multi-head self-attention layer with 8 attention heads. This initial attention layer allowed every token to attend to all others in the image sequence and modeled contextual dependencies across spatially distributed patches. To preserve the original representation, we added a residual connection followed by a layer normalization operation. This yielded an intermediate representation $F_1 \in \mathbb{R}^{256 \times 128}$.

However, this single-layer attention was seen as insufficient for modeling more complex long-range dependencies, such as posture-induced visual distortions. We stacked two Lightweight Transformer blocks to address this, where each was designed to refine the representation without incurring high computational cost. Each block then included multi-head self-attention, dropout, and a feed-forward sub-layer with expansion from 128 to 512 and back to 128 dimensions. The first block transformed F_1 into F_2 , and the second further refined it into F_3 . Finally, the refined tokens F_3 were passed through a position-wise feed-forward network to reweigh semantic features. We again used residual addition and normalization to ensure stability, producing the final enhanced image representation as shown in Equation (5):

$$\hat{F}_{img} = \text{LayerNorm}(F_3 + \text{FFN}(F_3)) \quad (5)$$

where FFN refers to the feed-forward network. This operation ensured that the learned image embeddings not only preserved spatial structure but also carried posture-specific attention cues.

3.2.3 Multimodal geometric correspondence module

While image tokens encode rich texture and appearance cues, pose tokens capture structured joint relationships. To

bridge this modality gap, we designed an enhanced Multimodal Geometric Correspondence Module (MGCM), which learns geometric correspondences using a cross-attention transformer architecture. Figure 5 shows the overall architecture of the proposed geometric correspondence module.

We began by projecting both modalities into a common space. The image tokens were first passed through a linear transformation followed by LayerNorm and GELU activation to form $F'_{img} \in \mathbb{R}^{256 \times d}$, where $d = 256$. Similarly, for the 33 anatomical keypoints, the coordinate embeddings were passed through a two-layer projection network with intermediate compression and re-expansion to produce $F'_{pose} \in \mathbb{R}^{33 \times d}$. Following this, we applied a cross-attention mechanism, where image tokens acted as (Q)ueries, and coordinate tokens served as both (K)eys and (V)alues. This allowed each visual token to dynamically attend to relevant joint embeddings and enable the model to align appearance cues with structural posture information. The feature attention output of this interaction is defined in Equation (6) as:

$$F_{attn} = \text{MultiHeadAttn}(Q = F'_{img}, K = F'_{pose}, V = F'_{pose}) \quad (6)$$

where $F'_{img} \in \mathbb{R}^{256 \times d}$ serves as the query matrix, and $F'_{pose} \in \mathbb{R}^{33 \times d}$ is used as both the key and value matrices. We then concatenated F'_{img} with F_{attn} to form a fused representation $F_{fused} \in \mathbb{R}^{1 \times 2d}$. To capture higher-order cross-modal interactions and enrich geometric understanding, we processed F_{fused} through 2 stacked Transformer layers. Each layer consisted of multi-head self-attention with 4 heads, feed-forward blocks with dimensionality expanded to $4d$, and residual normalization.

This transformer stack refined the fused representation

and modeled long-range dependencies across modalities. Finally, the output token was passed through a fusion head comprising a linear layer, LayerNorm, and GELU activation to generate the joint embedding $F_{\text{corr}} \in \mathbb{R}^{512}$, used for final classification. This operation is summarized as shown in Equation (7):

$$F_{\text{corr}} = \text{Fusion} \left\{ \text{Transformer} \left([F'_{\text{img}} \parallel F_{\text{attn}}] \right) \right\} \quad (7)$$

The module ensured the model was sensitive to the geometric interplay between joint positions and visual appearance by aligning visual and structural cues through cross-attention and subsequent refinement. This representation was then passed to the classification head for posture risk prediction.

4 Results

In this section, we present a comprehensive evaluation of the constructed MusDis-Sports dataset along with our proposed ViSK-GAT model for musculoskeletal risk assessment.

4.1 Evaluation metrics

To assess the performance of our proposed multimodal posture risk classification model, we employed a comprehensive set of evaluation metrics, including accuracy, precision, recall (sensitivity), and F1-score, as defined in Equations (8)-(11):

$$\text{Accuracy} = \frac{TP + TN}{TP + TN + FP + FN} \quad (8)$$

$$\text{Precision} = \frac{TP}{TP + FP} \quad (9)$$

$$\text{Recall} = \frac{TP}{TP + FN} \quad (10)$$

$$\text{F1-score} = 2 \cdot \frac{\text{Precision} \cdot \text{Recall}}{\text{Precision} + \text{Recall}} \quad (11)$$

where TP, TN, FP, and FN represent true positive, true negative, false positive, and false negative, respectively. In addition to these metrics, we also calculated the Matthews Correlation Coefficient (MCC) and Cohen’s Kappa coefficient. MCC measures classification quality across all confusion matrix categories, with values ranging from -1 (total disagreement) to +1 (perfect prediction). The unweighted Cohen’s Kappa (κ) quantifies agreement between predicted and true labels, adjusted for chance, where $\kappa = 1$ indicates perfect agreement and $\kappa = 0$ indicates random agreement. The metrics are defined in Equations (12), and (13), respectively:

$$\text{MCC} = \frac{TP \cdot TN - FP \cdot FN}{\sqrt{(TP + FP)(TP + FN)(TN + FP)(TN + FN)}} \quad (12)$$

$$\kappa = \frac{p_o - p_e}{1 - p_e} \quad (13)$$

where p_o is the observed agreement, and p_e is the expected agreement by chance. To quantify the numeric deviation in prediction, we computed the Root Mean Squared Error (RMSE) of the predicted probability distribution and the corresponding Mean Absolute Error (MAE) of the predicted probability distribution. These metrics measure the average deviation of the model’s predicted probability vector from the one-hot encoded ground truth label, providing insight into the model’s calibration and confidence in its predictions. The metrics are defined in Equations (14) and (15), respectively:

$$\text{RMSE} = \sqrt{\frac{1}{n} \sum_{i=1}^n \|\hat{p}_i - y_i\|_2^2} \quad (14)$$

$$\text{MAE} = \frac{1}{n} \sum_{i=1}^n \|\hat{p}_i - y_i\|_1 \quad (15)$$

where n is the number of samples, \hat{p}_i is the predicted probability vector (from the softmax output) for the i^{th} sample, and y_i is the one-hot encoded ground truth vector. In addition to these metrics, we further analyze the model’s behavior across the posture risk levels using class-wise diagnostic metrics, namely Negative Predictive Value (NPV), False Positive Rate (FPR), False Discovery Rate (FDR), and False Negative Rate (FNR).

4.2 Training analysis

All experiments were conducted using an NVIDIA GeForce RTX 3060 GPU with 12GB of VRAM in a CUDA 12.6 environment. The system was powered by an AMD Ryzen 5 5600X processor with 12 threads clocked at 3.7 GHz. The software environment included Python 3.12.9, PyTorch 2.6.0+cu126, and cuDNN 90501.

The training process was carried out using a supervised approach on the proposed multimodal dataset. The full dataset contained image-coordinate pairs annotated with REBA-based posture risk labels. The dataset was divided into 70% training, 10% validation, and 20% testing sets. We trained our multimodal model for 100 epochs using a batch size of 16. The optimizer used was AdamW with a weight decay of 1×10^{-5} to prevent overfitting. To improve learning dynamics, we used the OneCycleLR learning rate scheduler. This scheduler started with a low learning rate, gradually increased to a peak, and then decreased again over the course of training. The peak learning rate was set to 3×10^{-4} , with a warm-up over 10% of the epochs and a final decay according to a div factor of 1000. The model was trained on the resized (224×224) image data using a categorical cross-entropy loss function. At the end of training, the model achieved a training loss of 0.0007 and a training accuracy of 95.97% in the final epoch.

4.3 Classification assessment

To evaluate the performance of the proposed multimodal model, we assessed its ability to classify REBA scores based on posture. Our dataset includes a total of eight classes, each corresponding to a discrete REBA score ranging from 1 to 8. These labels were derived by analyzing the joint angles and positional configurations following the standard ergonomic assessment protocol [10].

4.3.1 Class-wise performance

The model demonstrates consistently strong classification ability across all REBA classes, with F1-scores ranging from 88% to 99%. Table 2 summarizes these per-class performance metrics.

Table 2: Class-wise precision, recall, F1-score, and specificity for REBA classification.

Class	Precision	Recall	F1-score	Specificity
Class 1	95.85%	98.11%	96.97%	99.43%
Class 2	88.46%	90.20%	89.32%	98.06%
Class 3	91.25%	91.63%	91.44%	98.65%
Class 4	89.47%	87.70%	88.58%	98.31%
Class 5	95.49%	97.80%	96.63%	99.30%
Class 6	96.07%	94.82%	95.44%	99.43%
Class 7	98.79%	98.78%	98.78%	99.88%
Class 8	98.98%	99.49%	99.23%	99.88%

Notably, classes such as class 1 (low risk) and classes 7–8 (high risk) show the highest performance, with F1-scores of 96.97%, 98.78%, and 99.23%, respectively. The specificity for these classes exceeds 0.99, indicating the model is very effective at ruling out incorrect classifications for extreme-risk postures.

In contrast, classes 2 and 4 exhibit comparatively lower F1-scores of 89.32% and 88.58%, respectively, as these moderate-risk classes contain more ambiguous or transitional postures, which increase confusion with adjacent categories. We note that precision for class 2 is the lowest overall (88.46%), and recall for class 4 is the lowest (87.70%), suggesting these classes are the most challenging for the model. We also analyzed the multiclass ROC curves to further investigate the model’s discriminative ability across the eight REBA classes. As shown in Figure 6 (left), the model shows excellent class separability, with most classes achieving an AUC of 1.0. Classes 2 and 3 scored slightly lower AUCs of 0.99, while class 4 recorded an AUC of 0.98. This observation is further supported by the confusion matrix in Figure 6 (right).

4.3.2 Overall evaluation

The model demonstrates superior musculoskeletal risk classification with an accuracy approaching 94%. However,

because accuracy alone can be misleading in multiclass settings, especially if class distribution is imbalanced, we further consider Cohen’s Kappa and the Matthews Correlation Coefficient (MCC), both of which are 93%. These metrics adjust for chance agreement and class imbalance, respectively. These low values indicate that the model’s predicted probability distributions are highly confident and closely aligned with the true labels, even for misclassified samples. The overall predicted probability distribution and result metrics are presented in Table 3.

Table 3: Overall classification metrics along with predicted error probability distribution of the proposed model.

Metric	Value
Accuracy	93.89%
Cohen’s Kappa	93.00%
Matthews Correlation Coefficient	93.00%
RMSE	0.1205
MAE	0.0156

4.3.3 Secondary error analysis

To identify where misclassifications are concentrated in the experiment, we examined Negative Predictive Value (NPV), False Positive Rate (FPR), False Discovery Rate (FDR), and False Negative Rate (FNR) for each class.

Table 4: Class-wise values for Negative Predictive Value (NPV \uparrow), False Positive Rate (FPR \downarrow), False Discovery Rate (FDR \downarrow), and False Negative Rate (FNR \downarrow) for REBA classification.

Class	NPV	FPR	FDR	FNR
Class 1	0.9975	0.0057	0.0415	0.0189
Class 2	0.9838	0.0194	0.1154	0.0980
Class 3	0.9872	0.0135	0.0875	0.0837
Class 4	0.9736	0.0169	0.1053	0.1565
Class 5	0.9968	0.0070	0.0451	0.0210
Class 6	0.9924	0.0057	0.0393	0.0517
Class 7	0.9988	0.0012	0.0121	0.0121
Class 8	0.9994	0.0012	0.0102	0.0051
<i>Average</i>	0.9912	0.0088	0.0570	0.0558

As seen in Table 4, classes 7 and 8 show exceptional values, with FNRs of 0.0121 and 0.0051, and FDRs below 0.011, which means that these high-risk cases are both rarely missed and rarely falsely predicted. In contrast, class 4 has the highest FNR at 0.1565, which indicates that it is the most commonly missed class. On average, the model scored 0.9912, 0.0088, 0.0570, and 0.0558 for NVP, FPR, FDR, and FNR, respectively.

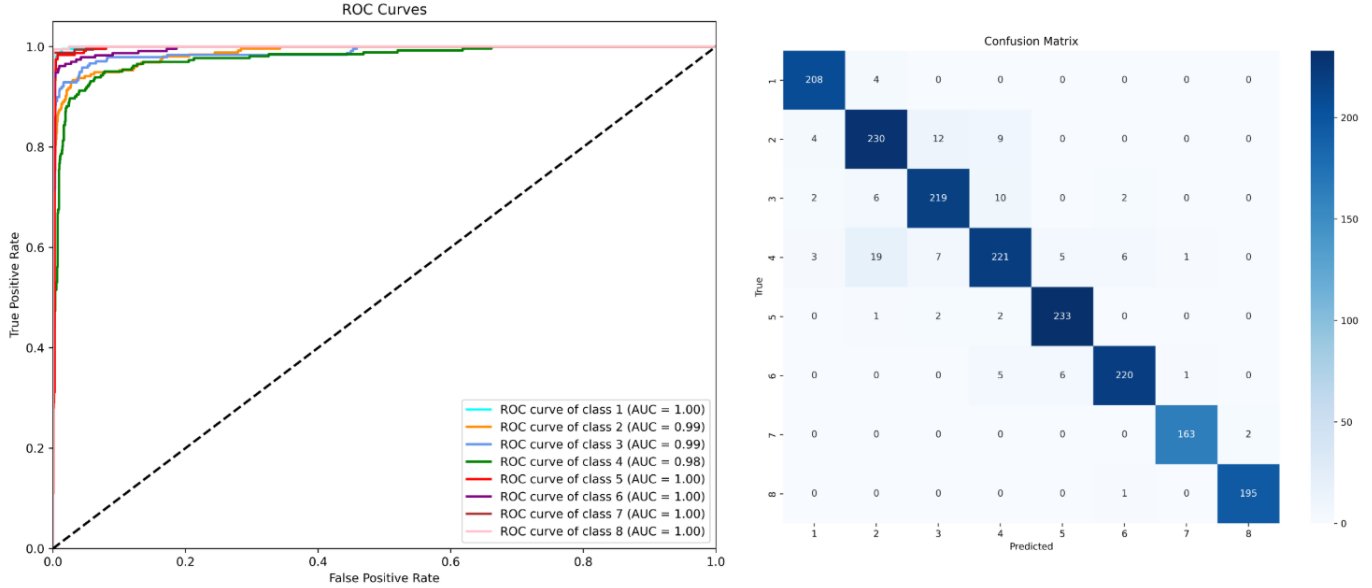


Figure 6: Left: Multiclass ROC curves for the eight REBA classes. Most classes achieve an AUC of 1.0, indicating excellent separability. Classes 2 and 3 scored 0.99, while class 4 scored 0.98. Right: Normalized confusion matrix showing classification performance across REBA classes. The strong diagonal pattern indicates high accuracy and minimal misclassification.

4.4 Comparison with existing studies

To contextualize the performance of our proposed system, we compared our proposed model (see Table 5) against existing state-of-the-art methods for posture risk assessment across various ergonomic scoring systems, including REBA, RULA, and OWAS. Here, RULA (Rapid Upper Limb Assessment) focuses on evaluating upper body postures; OWAS (Ovako Working posture Analysis System) targets whole-body posture in industrial settings; and REBA (Rapid Entire Body Assessment) provides a comprehensive evaluation of full-body postural risks.

Previous studies have shown promising results in ergonomic risk assessment using methods like RULA and OWAS. For instance, Li et al. [21] achieved 93% accuracy with RULA-based assessment, while Seo et al. [23] reported up to 90% accuracy using OWAS. However, relatively few approaches have focused on REBA-based classification, which accounts for a wider range of whole-body postural factors. Notably, Doong et al. [45] reported 76.1% accuracy for REBA-based posture classification. Although a few studies [25, 26, 37] have incorporated multimodal data with sensor-based inputs, applications in the sports environment remain largely unexplored. In contrast, our proposed multimodal framework significantly improves upon this baseline, achieving 93.89% accuracy in REBA classification. This is a substantial advancement in ergonomic risk evaluation, especially given REBA’s more detailed and comprehensive scoring system.

4.5 Comparison with state-of-the-art models

To evaluate the effectiveness of our proposed multimodal framework, we conducted a comprehensive comparison against standard deep learning models widely used as image feature extractors.

Given the multimodal nature of our dataset, we used each of the CNN backbone models for image feature extraction, while we processed the coordinate data using a multi-layer perceptron (MLP). The MLP consisted of stacked fully connected layers with ReLU activation, layer normalization, and dropout. Features from both modalities were then fused via concatenation, followed by a shared classification head to predict the REBA posture risk score. We kept this configuration intentionally consistent across all models to fairly assess the impact of different image backbones while holding the rest of the pipeline unchanged. Table 6 summarizes the training and validation accuracy and loss values for each configuration.

From the results, deeper models like ResNet101 and DenseNet121 demonstrate better performance compared to earlier architectures such as VGG16 or MobileNetV2. However, all these backbone combinations were performed below our proposed model. The best-performing baseline achieved 88.44% validation accuracy, while our method reached 93.66%. The lower training losses and higher validation scores of our model suggest more effective learning and generalization, due to the improved feature interaction

Table 5: Comparison of the proposed ViSK-GAT framework with prior studies in ergonomic posture risk assessment. The table highlights key methodological attributes, including the use of sensors, multimodal data fusion, and the ergonomic scoring system (REBA, RULA, OWAS).

Reference	Model	Dataset	Sensor-free	Multimodal	Accuracy	Assessment
Li et al. [21]	CNN-based	Collected	✓	✗	93.00%	RULA
Yan et al. [32]	Multimodal	Collected	✓	✓	89.20%	OWAS
Seo et al. [23]	SVM	Collected	✓	✗	89.00%	OWAS
Xiahou et al. [25]	MLP					
	RNN	Collected	✗	✓	90.00%	N/A
	LSTM					
Zhao et al. [26]	Multimodal	Collected	✗	✓	95.00%	N/A
Qi et al. [37]	Multimodal	Collected	✗	✓	89.76%	N/A
Doong et al. [45]	CNN-based	Public	✓	✗	76.10%	REBA
ViSK-GAT (ours)	Multimodal	Constructed	✓	✓	93.89%	REBA

Table 6: Comparison of our proposed multimodal model with various standard image feature extractor backbones combined with an MLP for coordinate data.

Backbone	Val Accuracy	Val Loss	Test Accuracy	Test Loss
VGG16	83.04%	0.6985	83.13%	0.7273
VGG19	84.12%	0.6844	84.20%	0.6911
ResNet50	87.81%	0.5981	87.75%	0.6746
ResNet101	88.44%	0.5832	88.39%	0.5812
InceptionV3	87.03%	0.6114	87.02%	0.6105
Xception	88.06%	0.5908	88.13%	0.5909
EfficientNet-B0	87.45%	0.6043	87.42%	0.6129
MobileNetV2	84.25%	0.6732	84.23%	0.6714
DenseNet121	88.12%	0.5925	88.06%	0.5947
ViSK-GAT (ours)	93.66%	0.4376	93.89%	0.4808

between modalities enabled by our FGAM and MGCM components. This comparison shows that while traditional CNN backbones provide a solid baseline, they are not sufficient on their own when dealing with multimodal inputs. Our model, designed specifically for this type of data, handles the interaction between visual and pose features more effectively.

4.6 Ablation studies

4.6.1 Module configurations

Starting from a baseline model that used simple concatenation of image and coordinate features without any dedicated enhancement modules, we first introduced Residual Blocks (ResB) into the image encoder, which resulted in an improvement in the F1-score of +0.0316 compared to the baseline (denoted as $\Delta F1$); along with an increase of +0.024 in Cohen’s κ . This improvement is attributed to the deeper hierarchical representations enabled by residual connections, which help preserve low-level spatial details while allowing effective gradient flow. Building on that, we

incorporated the Fine-Grained Attention Module (FGAM), which resulted in a $\Delta F1$ of +0.0501 and a κ gain of +0.044 compared to the baseline. FGAM allows the model to perform local, token-level attention between image patches and skeletal keypoints, rather than treating the modalities globally. Followed by FGAM, we added the Multimodal Geometric Correspondence Module (MGCM) module to the model, which led to the best results with a $\Delta F1$ of +0.0673 and κ improvement of +0.063 over the baseline. MGCM applies transformer-based cross-attention to explicitly model geometric relationships between modalities. Table 7 details the contribution of each key module to the model.

4.6.2 Hyperparameter Configurations

We conducted an extensive ablation study of 12 different experiments (Exp.) to evaluate the impact of various training hyperparameters on our multimodal posture classification model. The parameters tested include learning rate, batch size, weight decay, optimizer type, gradient clipping threshold, label smoothing, and loss functions.

Table 7: Ablation of key architectural modules. Performance improves incrementally with the addition of ResB, FGAM, and MGCM.

Modules	ResB	FGAM	MGCM	F1-score	Cohen’s κ	Δ F1 from Baseline
Baseline	✗	✗	✗	0.8712	0.867	N/A
+ ResBlocks	✓	✗	✗	0.9028	0.891	+0.0316
+ FGAM	✓	✓	✗	0.9213	0.911	+0.0501
+ MGCM (ViSK-GAT)	✓	✓	✓	0.9385	0.930	+0.0673

Table 8: Ablation study on training hyperparameters: learning rate (LR), batch size, weight decay, optimizer, gradient clipping threshold (Clip), label smoothing (L/ Smooth), and loss function (Loss). Training inference time is reported in minutes per epoch (Inf. Time). Best values in the training accuracy and loss are presented in bold, and the selected configuration for our final training is highlighted.

Exp	LR	Batch	Weight Decay	Optimizer	Clip	L/ Smooth	Loss	Inf. Time	Loss	Accuracy
1	1e-3	32	1e-3	Adam	1.0	0.1	CrossEntropy	~2:13	0.0018	0.9323
2	1e-4	16	1e-4	Adam	1.0	0.1	Focal	~1:45	0.0042	0.9080
3	2e-4	32	1e-5	SGD	0.5	0.1	Focal	~0:50	0.0060	0.9162
4	4e-4	16	1e-5	Adam	1.0	0.2	CE + Focal	~1:57	0.0014	0.9365
5	3e-4	16	1e-5	AdamW	1.0	0.1	CrossEntropy	~1:34	0.0007	0.9597
6	3e-4	32	1e-4	Adam	2.0	0.1	CrossEntropy	~0:51	0.0017	0.9284
7	4e-4	16	1e-4	AdamW	1.0	0.1	Focal	~1:50	0.0010	0.9522
8	3e-4	8	1e-5	Adam	1.0	0.1	CrossEntropy	~2:40	0.0021	0.9995
9	4e-4	32	1e-5	AdamW	1.0	0.1	CE + Focal	~1:10	0.0018	0.9945
10	3e-4	32	1e-5	AdamW	0.5	0.2	CrossEntropy	~0:58	0.0012	0.9391
11	4e-4	16	1e-4	Adam	1.0	0.1	CrossEntropy	~1:35	0.0015	0.9230
12	3e-4	8	1e-5	SGD	1.0	0.1	CE + Focal	~2:20	0.0050	0.9042

Experiments using adaptive optimizers such as Adam and AdamW generally outperformed SGD-based variants in both convergence and generalization. For example, while Exp. 3 (SGD) showed fast per-epoch times, but it struggled with higher losses. AdamW was more stable than vanilla Adam; as seen in Exp. 5 and Exp. 7, it contributed to smoother training dynamics and better generalization. The batch size of 16 proved to be an effective middle ground; configurations using larger batches (e.g., Exps. 1, 6, 9) trained faster but were slightly less robust, while smaller batches (Exps. 8, 12) led to very high training accuracy but also to signs of overfitting.

In terms of loss functions, standard CrossEntropy consistently performed well, whereas the combination with Focal loss (Exps. 4, 9, 12) slightly enhanced robustness in some cases but incurred longer training times. Using Focal loss alone (Exps. 2, 3, 7) helped with class imbalance to some extent, but was sensitive to the choice of optimizer. Moderate label smoothing (0.1) proved sufficient across most runs, while higher smoothing (0.2 in Exps. 4, 10) only offered marginal benefit. Similarly, clipping gradients above 1.0 (Exp. 6) led to reduced regularization and poorer generalization. Exp. 5, which employed a learning rate of 3e-4, AdamW, batch size 16, and CrossEntropy loss with 0.1 smoothing and clipping of 1.0, offered the best trade-off

accuracy and achieved the lowest training loss among all of the settings. Table 8 summarizes these configurations, along with corresponding training times per epoch, training and validation losses, and accuracies.

4.6.3 Features fusion

To further validate our architecture, we compared ViSK-GAT against standard multimodal fusion baselines, holding the training data and hyperparameters constant. As shown in Table 8, simple fusion strategies like early and late fusion perform poorly, as they cannot model complex interactions. A standard cross-attention baseline performs better but is still outperformed by ViSK-GAT. This demonstrates that the specific, sequential refinement of FGAM followed by the geometric alignment of MGCM provides a significant advantage over a naive cross-modal approach. The detailed findings are reported in Table 9.

4.6.4 Model complexity analysis

We conducted a comprehensive analysis of our model’s architectural footprint (see experimental hardware configuration in Section 4.2) to assess its suitability for real-world applications. The complete model comprises a total of 5.8 million parameters. The model requires 22.8 MB for trainable

Table 9: Ablation of the fusion module. The results are compared with existing early fusion, late fusion, and the standard transformer encoder fusion strategies.

Strategy	Fusion Method	Accuracy	F1-Score
Early Fusion	Pixel-coordinate concatenation at input	71.31%	68.91%
Late Fusion	Concatenation of final image/pose features	84.23%	83.01%
Cross-Attention	Standard transformer encoder fusion	88.77%	86.51%
ViSK-GAT (ours)	FGAM + MGCM	93.89%	93.85%

parameters and only 231 KB for non-trainable components, which results in a compact memory footprint suitable for various hardware platforms.

Table 10: Computational profile of the proposed ViSK-GAT model in terms of the major modules, including the Fine-Grained Attention Module (FGAM), and the Multimodal Geometric Correspondence Module (MGCM).

Component	Parameter	Trainable	Non-Trainable
Image Encoder	3.5 M	14.2 MB	121 KB
Coordinate Encoder	0.1 M	0.4 MB	8 KB
FGAM	1.2 M	4.8 MB	63 KB
MGCM	0.9 M	3.2 MB	39 KB
Classification Head	0.1 M	0.2 MB	0 KB
Total	5.8 M	22.8 MB	231 KB

The model demonstrated efficient training processing a full epoch in 1:34 minutes (see inference details in Table 8). The inference speed was measured at 8.2 milliseconds per frame, which translates to a processing rate of 122 frames per second. As detailed in Table 10, the efficient training time, compact memory footprint, and rapid inference speed demonstrate that the model is computationally feasible for both development and deployment phases in real-time monitoring and assessment.

5 Discussion

In this work, our objective was to improve the classification of musculoskeletal risk in sports by addressing key limitations in current posture assessment methods: poor integration of visual and skeletal data and lack of adaptability to sports postures. We proposed ViSK-GAT, a multimodal deep learning framework featuring a hybrid architecture that integrates residual and transformer blocks, along with two novel modules: a Fine-Grained Attention Module (FGAM) for refined feature interaction and a Multimodal Geometric Correspondence Module (MGCM) for better alignment between image and coordinate features. Furthermore, we introduced the MusDis-Sports dataset to support multimodal REBA-based classification in athletic settings.

We used the REBA scoring framework in our classification task to ensure ergonomic relevance and interpretability.

To create a system capable of scalable deployment in diverse athletic environments, we based our analysis on 2D skeletal coordinates extracted using MediaPipe. This approach was strategically chosen because it allows the model to operate on standard monocular video, which is vastly more accessible and practical in real-world sports settings than complex, laboratory-bound 3D motion capture systems. From the 33 extracted 2D keypoints, we computed joint angles using cosine and slope-based methods. These angles were then mapped to region-specific REBA posture scores, which were combined using standard REBA lookup tables [46] to compute a final risk score. While this 2D approximation introduces a known source of variation compared to a 3D biomechanical analysis, it provides a consistent and computationally efficient proxy for postural stress. Based on these scores, each sample was classified into one of eight discrete REBA risk classes, with higher class numbers indicating higher ergonomic risk.

To evaluate the contribution of each component to our architecture, we conducted stepwise ablation experiments, beginning with a baseline model that concatenated visual and skeletal features. As we incrementally incorporated residual blocks, the Fine-Grained Attention Module (FGAM), and the Multimodal Geometric Correspondence Module (MGCM), we observed consistent and significant improvements in performance. The complete ViSK-GAT model achieved a +6.73% increase in the F1-score over the baseline, with a final test precision of 93.86%, an F1-score of 93.85%, and Cohen’s Kappa of 0.93. These results reflect not only the effectiveness of our architecture but also its methodological novelty. Unlike existing approaches that often rely on simple fusion strategies or treat visual and skeletal modalities in isolation, ViSK-GAT introduces a structured multimodal integration pipeline that learns shared representations through attention-based mechanisms. MGCM enables explicit geometric alignment between image features and skeletal coordinates, allowing the model to understand spatial correspondences across modalities. This is complemented by FGAM, which enhances inter-modal interactions and supports fine-grained feature refinement. Together, these modules contribute to a unified architecture capable of modeling complex, dynamic postures in sports environments. ViSK-GAT represents a novel and effective paradigm for interpretable multimodal ergonomic analysis

by combining transformer-based attention, geometric reasoning, and domain-specific REBA scoring.

6 Limitations and future directions

Although our framework produced strong results, this study has a few limitations. We primarily focused on the critical task of classifying musculoskeletal risk from postural data (i.e., visual and skeletal coordinates) alone, using a REBA-inspired scoring system based solely on joint angles and body segment positions. This approach provides a robust foundation for vision-based postural analysis by isolating the most significant and visually discernible component of ergonomic risk.

It is important to note that the conventional protocol often incorporates additional modifiers for external load and repetitive activity. While these factors are important in a comprehensive risk assessment, they introduce variables that are often impossible to estimate accurately from visual data alone (e.g., the weight of a lifted object or the cumulative fatigue of an athlete). Our model’s design prioritizes high accuracy in the domain that computer vision can reliably address. Thus, the current model is more directly applicable to scenarios where risk is predominantly postural. The most promising direction for our future work will involve expanding the dataset to include more fine-grained metadata, such as sport type and athlete skill level, to enhance the model’s generalizability across diverse athletic disciplines in real-world scenarios.

7 Conclusion

In this study, we presented a multimodal deep learning framework (ViSK-GAT) to classify posture-related musculoskeletal risk in athletes by combining visual and skeletal features. Our key contributions include the design of a hybrid model architecture enhanced with a Fine-Grained Attention Module, which refines image-based cues, and a Multimodal Geometric Correspondence Module, which improves alignment between image and coordinate data using cross-attention. We also introduced the annotated MusDisSports dataset, labeled with REBA scores derived from joint angle calculations based on MediaPipe skeletal keypoints. The proposed model achieved a test precision of 93.86%, with an F1-score of 93.85% and Cohen’s Kappa of 0.93, and showed competitive and consistent performance at all levels of posture risk. Through detailed ablation studies, we showed that each architectural component contributed significantly to overall results, with the final configuration significantly outperforming the baseline models. In general, our framework provides an effective and interpretable solution for the classification of posture risk in sports environments. Its modular design and strong performance make it

a promising candidate for adaptation to broader ergonomic applications.

Declarations

Conflict of Interests: The authors declare that they have no financial conflicts of interest that could have influenced this work.

Ethics Approval and Consent to Participate. Not applicable.

Data and Code Availability: The dataset and code can be accessed through the following GitHub repository upon valid request for research purposes only: https://github.com/mak-raiaan/MusDis-Sports_Dataset.

References

- [1] S. Park, K. A. Rahaman, Y.-C. Kim, H. Jeon, and H.-S. Han, “Fostering tissue engineering and regenerative medicine to treat musculoskeletal disorders in bone and muscle,” *Bioactive materials*, vol. 40, pp. 345–365, 2024.
- [2] J. D. Hout and J. Ryu, “The association between musculoskeletal disorders and lead apron use in health-care workers: A systematic review and meta-analysis,” *Safety Science*, vol. 181, p. 106669, 2025.
- [3] A. B. Porto, A. N. Guimarães, and V. H. A. Okazaki, “The effect of exercise on postural alignment: A systematic review,” *Journal of Bodywork and Movement Therapies*, 2024.
- [4] A. Azadeh, I. M. Fam, M. Khoshnoud, and M. Nikafrouz, “Design and implementation of a fuzzy expert system for performance assessment of an integrated health, safety, environment (hse) and ergonomics system: The case of a gas refinery,” *Information Sciences*, vol. 178, no. 22, pp. 4280–4300, 2008.
- [5] F. Wang, X. Ao, M. Wu, S. Kawata, and J. She, “Explainable deep learning for semg-based similar gesture recognition: A shapley-value-based solution,” *Information Sciences*, vol. 672, p. 120667, 2024.
- [6] J. M. Muyor, E. Sánchez-Sánchez, D. Sanz-Rivas, and P. A. López-Miñarro, “Sagittal spinal morphology in highly trained adolescent tennis players,” *Journal of sports science & medicine*, vol. 12, no. 3, p. 588, 2013.
- [7] M. Grabara, “Comparison of posture among adolescent male volleyball players and non-athletes,” *Biology of sport*, vol. 32, no. 1, pp. 79–85, 2015.
- [8] Z. Bańkosz and K. Barczyk-Pawełec, “Habitual and ready positions in female table tennis players and their relation to the prevalence of back pain,” *PeerJ*, vol. 8, p. e9170, 2020.

- [9] E. Gawel and A. Zwierzchowska, "Effect of compensatory mechanisms on postural disturbances and musculoskeletal pain in elite sitting volleyball players: preparation of a compensatory intervention," *International journal of environmental research and public health*, vol. 18, no. 19, p. 10105, 2021.
- [10] S. Hignett and L. McAtamney, "Rapid entire body assessment (reba)," *Applied ergonomics*, vol. 31, no. 2, pp. 201–205, 2000.
- [11] L. McAtamney and N. Corlett, "Rapid upper limb assessment (rula)," in *Handbook of human factors and ergonomics methods*. CRC Press, 2004, pp. 86–96.
- [12] P. Kivi and M. Mattila, "Analysis and improvement of work postures in the building industry: application of the computerised owas method," *Applied ergonomics*, vol. 22, no. 1, pp. 43–48, 1991.
- [13] W. Marras, W. Allread, D. Burr, and F. Fathallah, "Prospective validation of a low-back disorder risk model and assessment of ergonomic interventions associated with manual materials handling tasks," *Ergonomics*, vol. 43, no. 11, pp. 1866–1886, 2000.
- [14] A. Hulme, J. Thompson, K. L. Plant, G. J. M. Read, S. Mclean, A. Clacy, and P. M. Salmon, "Applying systems ergonomics methods in sport: A systematic review," *Applied Ergonomics*, vol. 80, pp. 214–225, 2019.
- [15] S. E. Kazemi, S. Savas, and L. Aydos, "Evaluation of ergonomic postures of physical education and sport science by REBA and its relation to prevalence of musculoskeletal disorders," *International Journal of Sport Culture and Science*, vol. 4, no. 3, pp. 260–266, 2016.
- [16] P. Gorce and J. Jacquier-Bret, "Musculoskeletal disorder risk assessment during the tennis serve: Performance and prevention," *Bioengineering*, vol. 11, no. 10, p. 974, 2024.
- [17] D. Colombini and E. Occhipinti, *Risk analysis and management of repetitive actions: a guide for applying the OCRA system (occupational repetitive actions)*. CRC Press, 2016.
- [18] J. Wang, Y. Chen, S. Hao, X. Peng, and L. Hu, "Deep learning for sensor-based activity recognition: A survey," *Pattern recognition letters*, vol. 119, pp. 3–11, 2019.
- [19] M. Guo, Y. Xia, J. Liu, Y. Zhang, M. Li, and X. Wang, "Wearable pressure sensor based on triboelectric nanogenerator for information encoding, gesture recognition, and wireless real-time robot control," *Advanced Functional Materials*, p. 2419209, 2025.
- [20] J. Zhao, E. Obonyo, and S. G. Bilén, "Wearable inertial measurement unit sensing system for musculoskeletal disorders prevention in construction," *Sensors*, vol. 21, no. 4, p. 1324, 2021.
- [21] L. Li, T. Martin, and X. Xu, "A novel vision-based real-time method for evaluating postural risk factors associated with musculoskeletal disorders," *Applied Ergonomics*, vol. 87, p. 103138, 2020.
- [22] W. Kim, J. Sung, D. Saakes, C. Huang, and S. Xiong, "Ergonomic postural assessment using a new open-source human pose estimation technology (openpose)," *International Journal of Industrial Ergonomics*, vol. 84, p. 103164, 2021.
- [23] J. Seo and S. Lee, "Automated postural ergonomic risk assessment using vision-based posture classification," *Automation in Construction*, vol. 128, p. 103725, 2021.
- [24] S. H. Doong, "Predicting postural risk level with computer vision and machine learning on multiple sources of images," *Engineering Applications of Artificial Intelligence*, vol. 143, p. 109981, 2025.
- [25] X. Xiahou, Z. Li, J. Xia, Z. Zhou, and Q. Li, "A feature-level fusion-based multimodal analysis of recognition and classification of awkward working postures in construction," *Journal of Construction Engineering and Management*, vol. 149, no. 12, p. 04023138, 2023.
- [26] X. Zhao and J. Zhou, "Fast recognition algorithm for human motion posture using multimodal bioinformation fusion," *Mathematical Problems in Engineering*, vol. 2022, no. 1, p. 9538295, 2022.
- [27] X. Zhang, J. Fan, T. Peng, P. Zheng, X. Zhang, and R. Tang, "Multimodal data-based deep learning model for sitting posture recognition toward office workers' health promotion," *Sensors and Actuators A: Physical*, vol. 350, p. 114150, 2023.
- [28] I. H. Lopez-Nava and A. Munoz-Melendez, "Wearable inertial sensors for human motion analysis: A review," *IEEE Sensors Journal*, vol. 16, no. 22, pp. 7821–7834, 2016.
- [29] M. C. Schall Jr, H. Chen, and L. Cavuoto, "Wearable inertial sensors for objective kinematic assessments: A brief overview," *Journal of occupational and environmental hygiene*, vol. 19, no. 9, pp. 501–508, 2022.
- [30] D. Kee, "Comparison of owas, rula and reba for assessing potential work-related musculoskeletal disorders," *International Journal of Industrial Ergonomics*, vol. 83, p. 103140, 2021.
- [31] R.-J. Dzung, H.-H. Hsueh, and C. Ho, "Automated posture assessment for construction workers," in *2017 40th International Convention on Information and Communication Technology, Electronics and Microelectronics (MIPRO)*. IEEE, 2017, pp. 1027–1031.
- [32] X. Yan, H. Li, C. Wang, J. Seo, H. Zhang, and H. Wang, "Development of ergonomic posture recognition technique based on 2d ordinary camera for construction hazard prevention through view-invariant features in 2d skeleton motion," *Advanced Engineering Informatics*, vol. 34, pp. 152–163, 2017.

- [33] J. Seo, R. Starbuck, S. Han, S. Lee, and T. J. Armstrong, “Motion data-driven biomechanical analysis during construction tasks on sites,” *Journal of Computing in Civil Engineering*, vol. 29, no. 4, p. B4014005, 2015.
- [34] M. Liu, S. Han, and S. Lee, “Tracking-based 3d human skeleton extraction from stereo video camera toward an on-site safety and ergonomic analysis,” *Construction Innovation*, vol. 16, no. 3, pp. 348–367, 2016.
- [35] H. Zhang, X. Yan, and H. Li, “Ergonomic posture recognition using 3d view-invariant features from single ordinary camera,” *Automation in Construction*, vol. 94, pp. 1–10, 2018.
- [36] M. Palash and B. Bhargava, “Emersk-explainable multimodal emotion recognition with situational knowledge,” *IEEE Transactions on Multimedia*, vol. 26, pp. 2785–2794, 2023.
- [37] P. Qi, D. Chiaro, and F. Piccialli, “Fl-fd: Federated learning-based fall detection with multimodal data fusion,” *Information fusion*, vol. 99, p. 101890, 2023.
- [38] J. Liu, W. Zhao, J. Li, C. Li, S. Xu, Y. Sun, Z. Ma, H. Zhao, and L. Ren, “Multimodal and flexible hydrogel-based sensors for respiratory monitoring and posture recognition,” *Biosensors and Bioelectronics*, vol. 243, p. 115773, 2024.
- [39] Sabaheeraki, “Sports-1m dataset,” <https://www.kaggle.com/datasets/sabaheeraki/sports-1m-dataset>, 2023.
- [40] Gpiosenka, “Sports classification,” <https://www.kaggle.com/datasets/gpiosenka/sports-classification>, 2022.
- [41] Sidharkal, “Sports image classification,” <https://www.kaggle.com/datasets/sidharkal/sports-image-classification>, 2022.
- [42] Aneesh10, “Cricket shot dataset,” <https://www.kaggle.com/datasets/aneesh10/cricket-shot-dataset>, 2022.
- [43] C. Lugaresi, J. Tang, H. Nash, C. McClanahan, E. Uboweja, M. Hays, F. Zhang, C.-L. Chang, M. G. Yong, J. Lee *et al.*, “Mediapipe: A framework for building perception pipelines,” *arXiv preprint arXiv:1906.08172*, 2019.
- [44] Z. Jiao, K. Huang, Q. Wang, G. Jia, Z. Zhong, and Y. Cai, “Improved reba: deep learning based rapid entire body risk assessment for prevention of musculoskeletal disorders,” *Ergonomics*, vol. 67, no. 10, pp. 1356–1370, 2024.
- [45] S. H. Doong, “Predicting postural risk level with computer vision and machine learning on multiple sources of images,” *Engineering Applications of Artificial Intelligence*, vol. 143, p. 109981, 2025.
- [46] T. Paillard, C. Costes-Salon, C. Lafont, and P. Dupui, “Are there differences in postural regulation according to the level of competition in judoists?” *British journal*